Infrasound monitoring of volcanoes to probe high-altitude winds

A. Le Pichon, E. Blanc, D. Drob, S. Lambotte, J.X. Dessa, M. Lardy, P. Bani, S. Vergniolle

Infrasound monitoring of volcanoes to probe high-altitude winds

A. Le Pichon,[1] E. Blanc,[1] D. Drob,[2] S. Lambotte,[3] J. X. Dessa,[4] M. Lardy,[5] P. Bani,[5] and S. Vergniolle[6]

Received 8 November 2004; revised 7 February 2005; accepted 2 March 2005; published 6 July 2005.

[1] Active volcanoes in the Vanuatu archipelago permanently generate infrasonic waves. Their monitoring over 1 year exhibits clear seasonal trends in the direction of arrival of the detected signals. From summer to winter the azimuth variation reaches 15°. This deviation is essentially due to the reversibility of the zonal stratospheric wind with season which strongly affects the deflection of the ray direction. A three-dimensional (3-D) ray-tracing modeling roughly explains the observed seasonal trend in the azimuth variation but underestimates its amplitude. The discrepancy between the measurements and the results of simulation is explained by undervalued wind speeds in the upper atmosphere. Infrasonic observations are used as input of an inversion scheme for adjusting the vertical structure of the wind in the upper stratosphere and mesosphere. It is shown that the mesospheric zonal winds are underestimated by at least 20 m/s throughout the year with differences reaching 50 m/s.

Citation: Le Pichon, A., E. Blanc, D. Drob, S. Lambotte, J. X. Dessa, M. Lardy, P. Bani, and S. Vergniolle (2005), Infrasound monitoring of volcanoes to probe high-altitude winds, *J. Geophys. Res.*, *110*, D13106, doi:10.1029/2004JD005587.

1. Introduction

[2] Infrasonic waves propagate in the atmosphere over very large distances in the waveguide formed by the atmosphere and its temperature gradients. Ducting is especially efficient in the ground to stratosphere and thermosphere waveguides. It can be reinforced or reduced by the high-altitude winds [*Georges and Young*, 1972]. As waves propagate in the upper atmosphere, the wave front characteristics reveal, in addition to information about the source, significant features of the vertical structure of the winds. The interpretation of these data motivated studies on sources of infrasonic waves and their propagation in the upper atmosphere. It has been proposed to retrieve the characteristics of high-altitude winds from naturally occurring geophysical phenomena such as the ocean swell [*Herron and Tolstoy*, 1968; *Rind and Donn*, 1975; *Rind*, 1978], chemical ground based explosions [*Bush et al.*, 1989; *Kulichkov*, 1992], or the Concorde supersonic aircraft [*Donn*, 1978]. Infrasound generated by the daily Concorde flights between North America and Europe have systematically been used to quantify wind effects in the seasonal azimuth deviations [*Le Pichon et al.*, 2002a]. The stratospheric duct during the winter months was well predicted and a consistent agreement between the observations and ray tracing calculations were obtained. However, the HWM/MSIS empirical atmospheric models [*Hedin*, 1991] used for this work did not sufficiently describe the highly variable tropospheric and stratospheric winds since large daily range of arrivals of several degrees were not well modeled.

[3] Volcanic eruptions are other unique sources for atmospheric studies [*Wilson and Forbes*, 1969]. Explosive eruptions quite often involve a pressure release suddenly uncorked at the top of the volcano. Explosive eruptions produce infrasound waves where hot gazes and rock fragments are ejected to form either acoustic or shock waves. Large explosive eruptions, such as Mt. St. Helens (USA, 1980) are able to excite gravity waves in the atmosphere as large mass and heat flux are suddenly emplaced [*Delclos et al.*, 1990; *Kanamori et al.*, 1994]. Basaltic eruptions also produce sound waves during Strombolian explosions [*Vergniolle et al.*, 2004]. The equivalent explosion yield is very variable from one volcano to another. It may range from few tens of pounds of TNT for the Arenal volcano (Costa Rica), up to few Mt for the Mount St. Helens eruption of 1980 [*Reed*, 1987; *Donn and Balachandran*, 1981], or the Pinatubo eruption of 1991 [*Tahira et al.*, 1996]. Volcanic eruptions also produce more continuous tremor waves. The origin could be an out burning of gas bubbles in the upper part of the magmatic column [*Ripepe et al.*, 1996]. Tremor infrasound can be observed up to distances of several thousands of kilometers from a volcanic eruption [*Liszka and Garcés*, 2002]. Recently, microbarometers have been used to estimate burst pressure and gas concentrations in explosive volcanic eruptions providing a description of the infrasound source [*Morrissey and Chouet*, 1997]. Infrasound from volcanic

[1]Laboratoire de Détection et de Géophysique, Département Analyse Surveillance Environnement, Commissariat à l'Energie Atomique, Bruyères-le-Châtel, France.
[2]E.O. Hulburt Center for Space Research, Naval Research Laboratory, Washington, D. C., USA.
[3]Ecole et Observatoire des Sciences de la Terre, Institut de Physique du Globe de Strasbourg, Strasbourg, France.
[4]Laboratoire de Géosciences Marines, Institut de Physique du Globe de Paris, Paris, France.
[5]Institut de Recherche pour le Développement, Noumea, New Caledonia.
[6]Laboratoire de Dynamique des Systèmes Géologiques, Institut de Physique du Globe de Paris, Paris, France.

0148-0227/05/2004JD005587

eruptions are then very valuable for a global atmospheric monitoring since infrasound can be generated over long duration, allowing investigations in the seasonal and diurnal fluctuations of the atmosphere.

[4] Such studies are now in expansion with the development of a network of 60 infrasound stations for the enforcement of the Comprehensive Nuclear-Test ban Treaty (CTBT). This network already allows a global Earth's coverage for infrasound monitoring. Compared to previous systems, the performances of this network are greatly improved with efficient array designs and the installation of sensitive microbarometers associated with robust noise reducer systems [*Vivas Veloso et al.*, 2002]. Furthermore, efficient algorithms for analyzing low-amplitude infrasonic coherent waves within noncoherent noise provide now a precise determination of the direction of arrival of low-amplitude signals.

[5] The main objective of this paper is to demonstrate the capability of measuring fine temporal wind fluctuations in the upper stratosphere and mesosphere thanks to a continuous monitoring of active volcanoes. Three volcanoes of the Vanuatu archipelago (New Hebrides islands) are selected. They are located to the north-northeast of the I22FR infrasound station (New Caledonia) at distances of ~500 km. First, simulations are carried out with a 3-D ray-tracing code associated with the NRL-G2S climatological database accounting for the highly variable tropospheric and stratospheric winds. The predicted azimuth deviations of the identified ray paths are then compared to the observations. Finally, infrasound observations are used as input of an inversion procedure to evaluate more precisely the vertical structure of the wind in range of altitude inaccessible to ground-based or satellite measurements.

2. Infrasound Monitoring of Volcanic Activity in Vanuatu

2.1. Geologic and Historical Background

[6] The Vanuatu archipelago, located in the South Pacific between New Caledonia and Fiji, is composed by more than 80 islands. The entire island chain owes its existence to the active volcanism resulting from the northeast ward directed subduction of the Australian Plate beneath the edge of the Pacific Plate [*Eissen et al.*, 1991; *Robin and Monzier*, 1994; *Simkin and Siebert*, 1994]. Although the large majority of volcanoes in that tectonic context produce an explosive activity with silicic magmas, magmas emitted around Vanuatu are largely basaltic. Consequently, eruptions are generally less violent because of the low magma viscosity.

[7] Most of the volcanic eruptions in Vanuatu are Strombolian or mild Vulcanian, sometimes resulting in huge expanses of thick ash. The four most active volcanoes of Vanuatu described below present various degrees in explosivity. The Lopevi volcano (16.50°S, 168.34°E, 1410 m high), whose activity was first reported in 1863 [*Warden*, 1963; *Lardy et al.*, 1999], produces pyroclastic flows as well as Strombolian and Vulcanian explosions [*Eissen et al.*, 1991; *Lardy et al.*, 1999]. It is one of the most active of the Central Islands of Vanuatu. It can also produce basaltic plumes, such as on 8 June 2003, with a height of 8 km above sea level (Global Volcanism program, USGS). Although basaltic plumes are rare events at Lopevi, they can occur during its 15–20 years period of activity, which is generally followed by 20–30 years of quiescence. Ambrym (16.25°S, 168.12°E, 1330 m high, ~10 km wide) is the most voluminous active volcano in Vanuatu. It produces the largest magma volume, with more than 50 eruptions reported since 1774 [*McCall et al.*, 1970; *Robin et al.*, 1993]. Although eruptions have been explosive in the past, the current activity consists in a lava lake; a cooler layer of magma slowly develops at the surface until that thin layer is disrupted by the arrival of large bubbles. During March 2004, the GVP/USGS reported an active lava lake within one of the summit craters and thunderous explosions. Yasur (19.52S, 169.42E, 360 m high), after 800 years of continuous activity [*McClelland et al.*, 1989], is now producing a series of explosions, whose intensity varies between Strombolian and mild Vulcanian. These are triggered by the sudden decompression of the inner magmatic gas, which expels magma fragments at the vent with large velocities. A huge variation in intensity and number of explosions exists, from 20 to 1300 per day (25 February 2003 to 8 July 2003) with a value of 500 in March 2004. The last one, Epi B, is a newly growing submarine volcano, whose explosions occur less than 50 m below the sea surface. It can produce layers of pumices over the sea surface with areas up to 1000 km^2.

2.2. Observations

[8] The I22FR infrasound array (16.26°S, 68.45°W), installed in New Caledonia, is part of the global infrasonic network of the International Monitoring System (IMS). Such a network provides an opportunity to monitor geophysical phenomena on a global scale [*Hedlin et al.*, 2002]. The I22FR station is composed of four microbarometers, 1 to 2.5 km apart. Each sensor is a MB2000 microbarometer that can measure both absolute and relative pressure. The MB2000 has been designed to operate from DC up to 27 Hz with an electronic noise level of 2 mPa RMS in the 0.02–4 Hz frequency band. With a sampling rate of 20 Hz, the expected numerical resolution at 1 Hz is of the order of 0.5° for the azimuth and 5 m/s for the horizontal trace velocity. In order to minimize pressure changes due to surface wind effects, each sensor is connected to an 18-m-diameter noise reducing system equipped with 32 inlet ports that significantly improves the detection capability above 1 Hz [*Alcoverro and Le Pichon*, 2005]. Since the beginning of its installation, the I22FR station continuously detects coherent infrasonic waves originating from three active volcanoes described above. The Lopevi and Ambrym volcanoes are situated at distances of 648 and 670 km from I22FR in the directions of 14.3° and 11.8° clockwise from north, respectively. The Yasur volcano is located at 399 km to the north-northeast (42.7°) of the station (Figure 1). This favorable setting allows an accurate determination of the acoustic wave front characteristics with signal-to-noise ratio frequently greater than one. Considering a nearly southward direction of propagation for Lopevi and Ambrym, it also makes easier the evaluation of the zonal wind model from the observed azimuth deviation.

[9] The wave parameters of the infrasonic waves are calculated with the progressive multichannel correlation

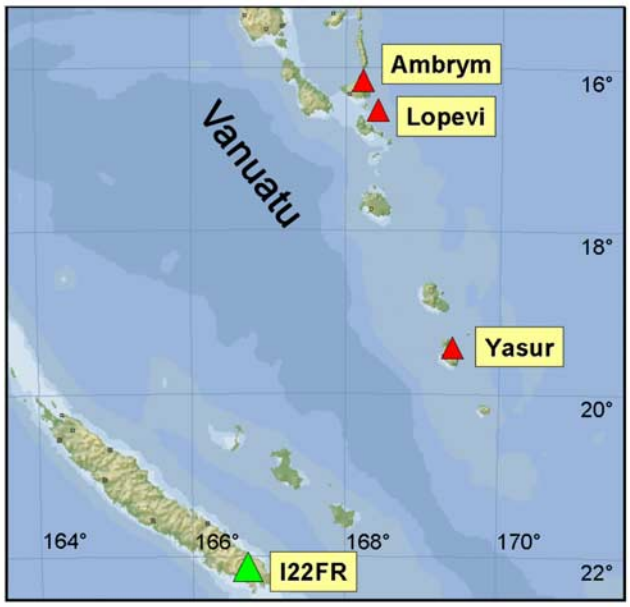

Figure 1. Geographic situation of the archipelago of Vanuatu in Oceania. The green triangle indicates the location of the I22FR infrasound station (New Caledonia). The red triangles indicate three active volcanoes.

method (PMCC) used as a real-time detector [*Cansi*, 1995]. This method, originally designed for seismic arrays, proved to be very efficient for infrasonic data and is well adapted for analyzing low-amplitude coherent waves within noncoherent noise [*Le Pichon et al.*, 2002b]. Figure 2 presents the results of continuous PMCC processing in the [0.1–4] Hz band from June 2003 to October 2004. Because of the geographic situation of I22FR, most of the detected infrasonic waves are produced by standing ocean waves near low-pressure systems in the south Pacific [*Garcés et al.*, 2004]. From 0.1 to 0.3 Hz, microbaroms are permanently observed and their monitoring over one year exhibits a clear seasonal trend correlated with changes in the stratospheric wind direction (blue dots in Figure 2). Above 0.5 Hz, for azimuths ranging from 0 to 50°, permanent detections from two distinct sources are observed (Figure 2b). Yellow dots are associated with detections from the Yasur volcano. These signals are observed from December 2003 to April 2004 with a dominant frequency greater than 1 Hz. Cyan dots indicate signals at lower frequency (~0.5 Hz) in the direction of Lopevi. From I22FR the difference in azimuth between Lopevi and Ambrym is less than 3°. Taking into account uncertainties due to the propagation, the discrimination of these two volcanoes becomes tricky. However, during the studied period, according to the GVP/USGS reports, Lopevi was the most active. As for microbaroms, seasonal changes in the bearings of these signals are noted. From austral summer to austral winter, the azimuth variations approach 8° and 15° for Yasur and Lopevi, respectively.

[10] Figures 3 and 4 present the results of the interactive PMCC analyses on typical waveforms from Lopevi and Yasur, with the same set of detection parameters. For both volcanoes, phase-aligned signals show quasi-monochromatic coherent wave trains with horizontal trace velocities ranging from 0.34 to 0.37 km/s. Peak-to-peak amplitudes are about 0.2 Pa for Lopevi and 40 mPa for Yasur. Distinct arrivals from Yasur are also observed. On 8 June 2003, the measured signals from Lopevi are associated with continuous gas release during the strong eruptions which occurred at that time. A plume rose into the atmosphere up to several kilometres. The dominant frequency of these waves is about 0.5 Hz (Figure 3b). In contrast, for Yasur, the measured frequency ranges generally from 2 to 4 Hz (Figure 4b). Eruptive activity at Yasur is very similar to Strombolian activity, hence corresponds to the regular breaking of overpressurized bubbles as large as the volcanic conduit [*Hagerty et al.*, 2000; *Vergniolle and Brandeis*, 1996]. We suggest that the difference in frequency between Yasur and Lopevi is mainly related to the source. Since infrasonic waves of higher frequency are subject to increased attenuation in the upper atmosphere, considering frequency greater than 1 Hz, thermospheric ducted waves from Yasur are not measurable at I22FR.

3. Propagation Modeling

3.1. Atmospheric Specifications

[11] A number of institutions worldwide build and maintain networks of ground-based weather stations and meteorology satellites. The resulting measurements are continuously assimilated into operational numerical weather prediction systems (NWP) via the combination of rigorous statistics and geophysical fluid models. However, forecasts mainly provide output for general consumption below 35 km. Consumer demand for specifications above 35 km is limited to the fact that it is difficult and expensive to make routine measurements above this altitude. Among the available empirical reference models, the Mass Spectrometer and Incoherent Radar Model (MSIS-90, NRL/MSISE-00) [*Hedin*, 1991; *Picone et al.*, 2002] and the Horizontal Wind Model (HWM-93) [*Hedin et al.*, 1996], provide time-dependent estimates of winds, temperatures, pressures, and major species concentrations. These models account for the major seasonal variations, daily solar tidal variability, and geomagnetic and solar forcing effects in the mesosphere and lower thermosphere (55 to 150 km). The represented geophysical variations in climatologies, however, can often be overshadowed by naturally occurring stochastic variations. For example, *Drob and Picone* [2000] showed that the HWM empirical model can underestimate the magnitude of the stratospheric wind jets by as much as 50 m/s over large spatial regions for extended periods of time. These errors are large enough to result in erroneous predictions of stratospheric ducting and can lead to erroneous interpretations of infrasound observations [*Drob et al.*, 2003]. To eliminate these climatological biases in the troposphere and stratosphere, the HWM/MSIS models can be combined with daily NWP data. The NRL-Ground to Space (NRL-G2S) semiempirical atmospheric specification system fuses operational NWP analysis with the HWM/MSIS climatologies. It provides a highly resolved, self-consistent, global and regional atmospheric specification that extends from 0 to 170 km for infrasound propagation calculations. The mathematical details and composite data sets are described in [*Drob et al.*, 2003]. A climatological database of G2S coefficients covering the time period

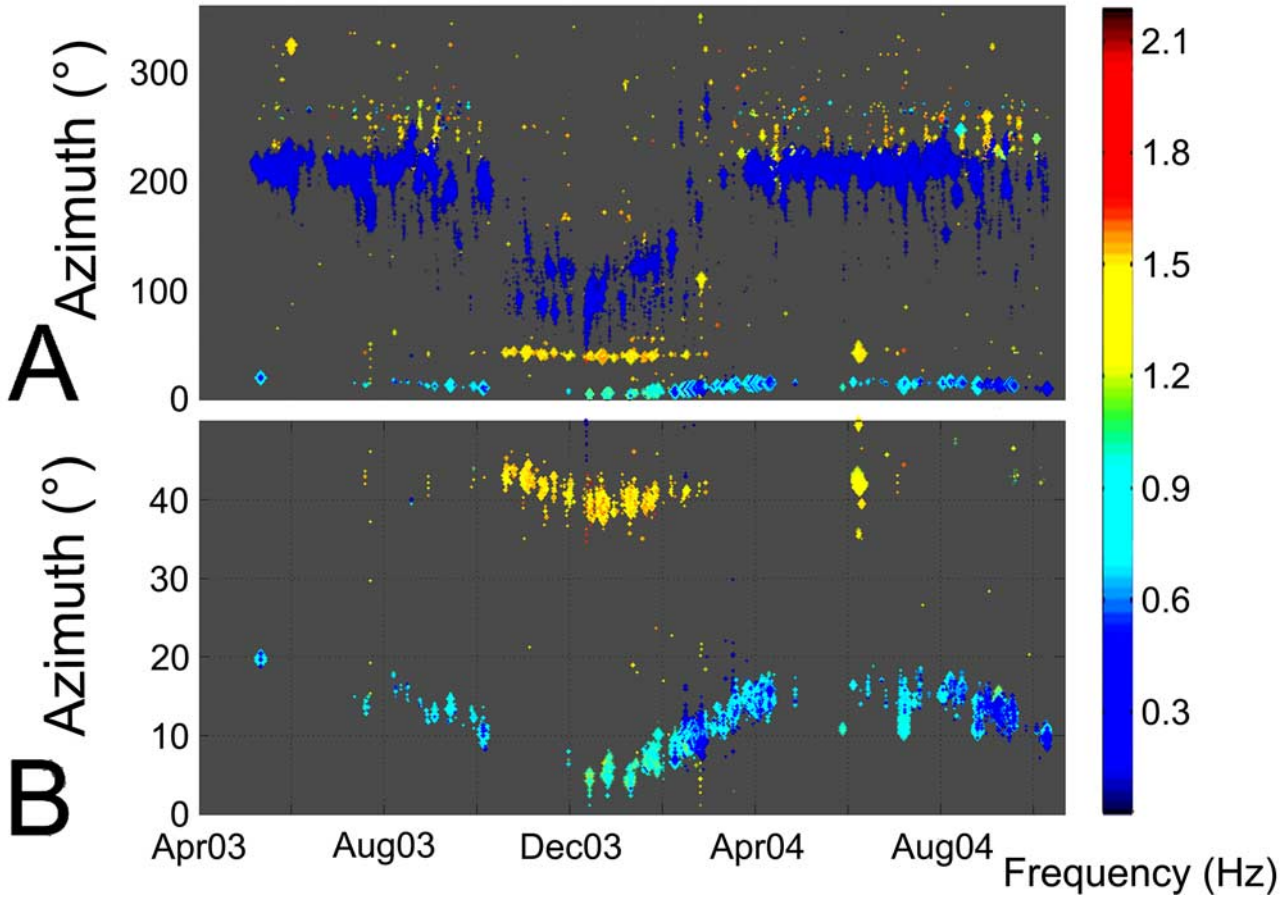

Figure 2. Results of the automatic PMCC processing in the [0.1–4] Hz band from June 2003 to October 2004. Each dot indicates detection of coherent infrasonic waves. Color refers to the dominant frequency. The size of the dot is related to the duration of the detection. (a) Azimuths ranging from 0° to 360°. (b) Zoom in azimuth emphasizing the detections related to the Lopevi and Yasur volcanoes.

1 January 2003 to April 2004, at 6-hour intervals with a truncated spectral resolution of ~2.0° was used for this study.

3.2. Propagation Modeling in Moving Medium

[12] On the basis of the asymptotic approximation of high-frequency infrasound waves, ray theory appears as a relevant technique for propagation modeling through the atmosphere. We consider that pressure perturbations are limited so that the motion of the atmospheric medium is ruled by the linearized hydrodynamic equations for a compressible fluid. This implies that the signal wavelengths are smaller than those of atmospheric property variations, a condition that is always fulfilled in practice. The propagation modeling is performed using the WASP-3D ray theory-based method [*Virieux et al.*, 2004]. Considering large propagation range, these equations take into account the ground elevation, the Earth's curvature, and also include the spatiotemporal variations of horizontal wind terms along the ray paths. From the implementation of the Hamiltonian function in spherical coordinates [*Jones et al.*, 1986], the equations describing the evolution of the ray canonical variables (slowness vectors, position and propagation time) are numerically solved by a second-order Runge-Kutta scheme. This formulation allows wind and sound speed variations in time and space during propagation, which is interesting for long propagation distances. For numerical integration, range-dependent atmospheric profiles are interpolated along the ray trajectory, in space with third-order cardinal B-spline functions, and linearly in time as needed.

[13] A paraxial approach for the amplitude computation is used. Considering small perturbations of the slowness vector and position around a central ray of reference, one can build neighboring rays termed as paraxial rays. This allows estimating in three dimensions the evolution of the cross section of a ray tube, hence giving the local amplitude of the signal [*Virieux and Farra*, 1991]. Because of the low particle density and nonlinear dissipation in the upper atmosphere, thermospheric returns are strongly attenuated at range of hundreds of kilometers with absorption increasing with frequency. In our simulations, the atmospheric absorption is integrated using range-dependent attenuation coefficients varying with the altitude, the frequency of the propagating wave and atmospheric parameters (gas composition, density, pressure, temperature and humidity). The classical and rotational relaxation losses dominate at high altitude whereas vibrational losses are the main process of absorption in the low part of the atmosphere (up to 60 km at 0.5 Hz). The coefficients used are those calculated by *Sutherland and Bass* [1996]. They provide a relevant

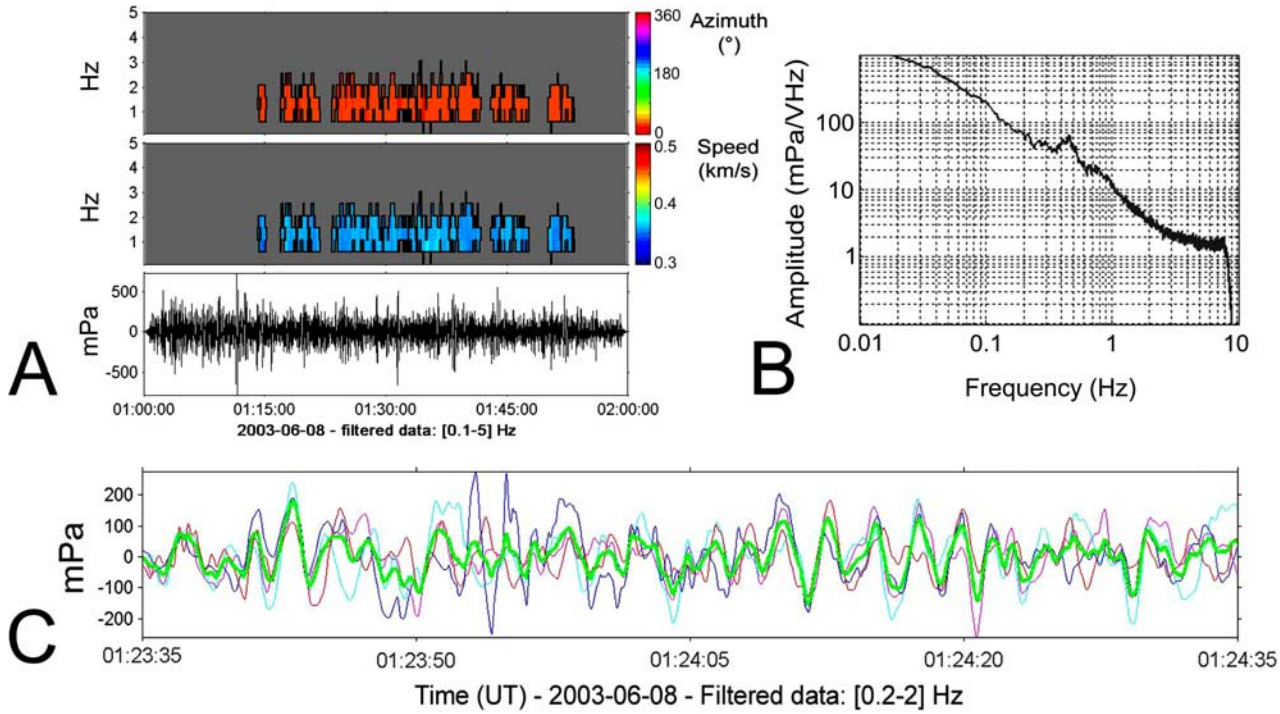

Figure 3. Results of PMCC calculation on typical signals recorded at I22FR from Lopevi. (a) Time/frequency representation of the horizontal trace velocity and azimuth. Values are given according to the color scales. The results are presented from 0.1 to 5 Hz in 10 equally spaced frequency bands. Azimuths are given clockwise from north. (b) RMS spectrum showing a maximum of energy of the signals between 0.4 and 0.5 Hz. (c) One minute of phase-aligned signals filtered between 0.2 and 2 Hz (stack in green).

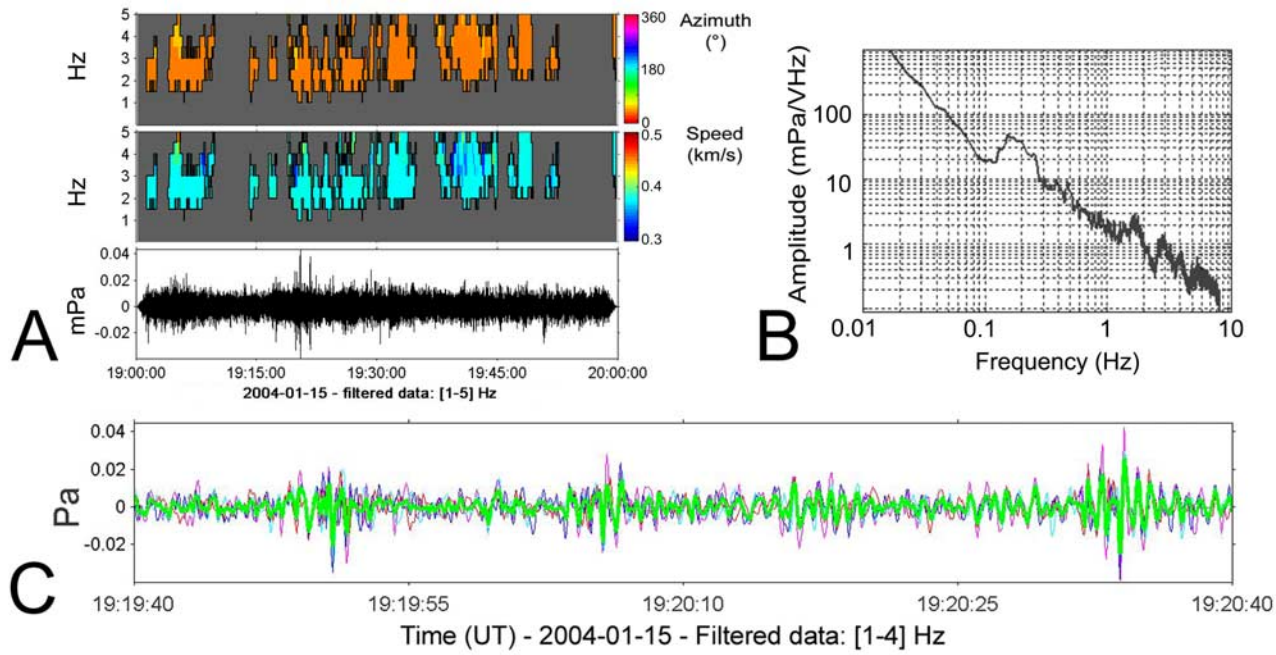

Figure 4. Results of PMCC calculation on typical signals recorded at I22FR from Yasur. (a) PMCC results. (b) RMS spectrum showing a maximum of energy of the signals. Above the microbaroms peak at 0.2 Hz, the maximum of energy of the signals ranges between 2 to 3 Hz. (c) One minute of phase-aligned signals filtered between 1 and 4 Hz.

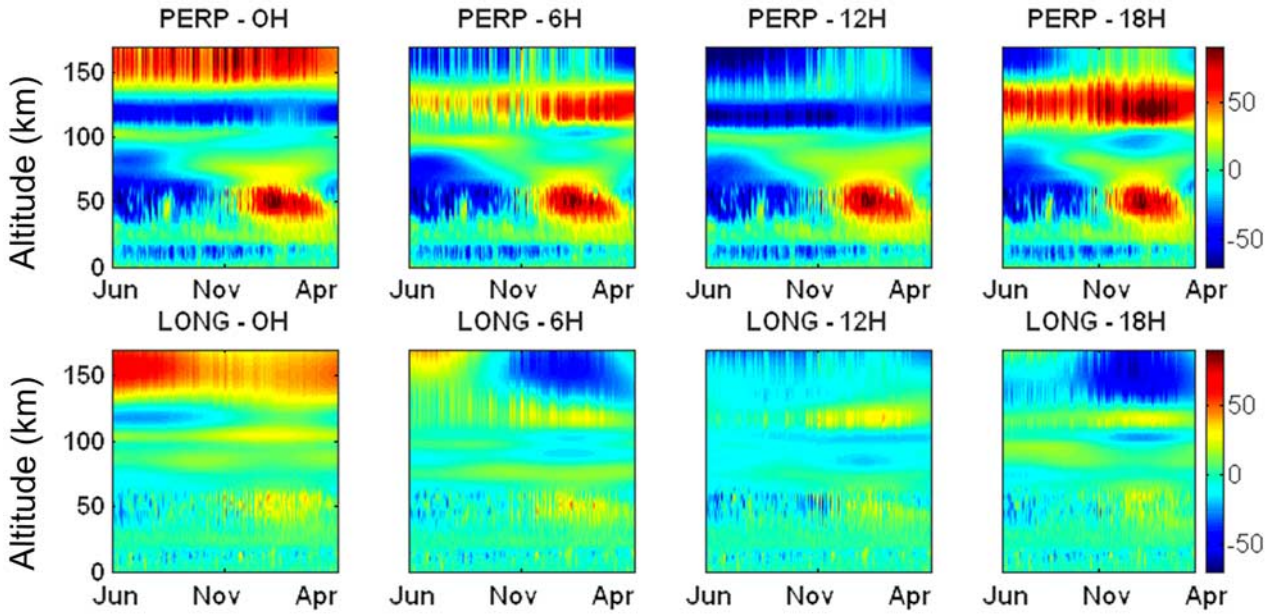

Figure 5. Seasonal and diurnal variations of the G2S wind models as a function of altitude. Wind profiles (speed in m/s) are averaged along the great circle between Lopevi and I22FR. They are given at intervals of 0000, 0600, 1200, and 1800 UTC perpendicular (PERP) and along (LONG) the direction of propagation from June 2003 to May 2004. Positive values are in the direction of propagation for the parallel component and to the right of the ray direction for the transverse component.

estimation of absorption for infrasonic waves propagating through the atmosphere by integrating classical absorption (diffusion and viscothermic losses) and relaxation losses (rotation and vibration) [*Greenspan*, 1959; *Evans et al.*, 1972; *Rind*, 1977; *Bass et al.*, 1995].

3.3. Simulating the Propagation

[14] For the simulations, the variability in time and space of the atmospheric profiles is taken into account. Simulations are first carried out using the HWM-93/MSIS-90 empirical models as input in WASP-3D. Then, in order to integrate assimilation of tropospheric and stratospheric winds up to 55 km, G2S atmospheric models are used. Figure 5 shows the seasonal and diurnal variations of the G2S wind models for infrasonic waves propagating from Lopevi to I22FR. Since the direction of propagation is nearly southward, the parallel and transverse wind components are mainly driven by the meridional (positive to the north) and zonal (positive to the east) winds, respectively. The transition in the stratospheric general circulation between the summer and winter is observed. Around and above the stratopause (altitude of 40–70 km), the zonal winds reverse in November and May. The daily tidal wind fluctuations in the upper atmosphere, with dominant periods of 24, 12, and 8 hours, are the direct result of the solar heating of water vapor, ozone, and other molecular species in the lower atmosphere which propagate vertically and grow in amplitude. These migrating solar tides are the main sources of daily variability in the mesosphere and thermosphere. Stochastic variability of medium- and large-scale gravity waves, as well as global-scale propagating planetary waves are of equal significance in the 55 to 120 km region, but are unfortunately irresolvable by today's observationally based global atmospheric specification systems.

[15] The atmospheric profiles are defined over a grid ranging from 164° to 170°E in longitude, 14° to 24°S in latitude, and 0 to 170 km in altitude (Figure 6a). On 8 June 2003, a maximum difference of ~50 m/s in the wind speed is found over this grid in the stratosphere (Figure 6b). Such a spatial variability persists throughout the year. Attenuation coefficients are interpolated from the atmospheric profiles given by the MSIS-90 model at each node of the grid. Simulations are carried out for infrasonic waves generated by the Lopevi and Yasur volcanoes, assuming a source at altitude of 1400 m and 400 m, respectively. Following a shooting procedure, simulations are then performed for values of ray parameters derived from the measured horizontal trace velocities. Twenty rays are launched with slowness values ranging from 2.6 to 3.0 s/km. Rays trajectory and amplitude are computed each day from June 2003 to April 2004 at 0, 6, 12 and 1800 UT. Only rays with bounces contained within a circle of radius 50 km around I22FR are selected. In the next section, the simulated results are compared to the observations.

4. Comparisons With Measurements: Results and Discussions

4.1. Seasonal Changes

[16] For both volcanoes, the observed seasonal azimuth deviation is well beyond its numerical resolution (~0.5°) and its uncertainty related to short timescale atmospheric variability (~2°). Depending on the strength of the transverse wind component along the ray path, the arrival direction does not correspond to the original launch direction (Figure 7a). A maximum azimuth deviation of ~10° is noted. As the propagation from Lopevi is nearly southward, the azimuth deviation is essentially due to the reversibility

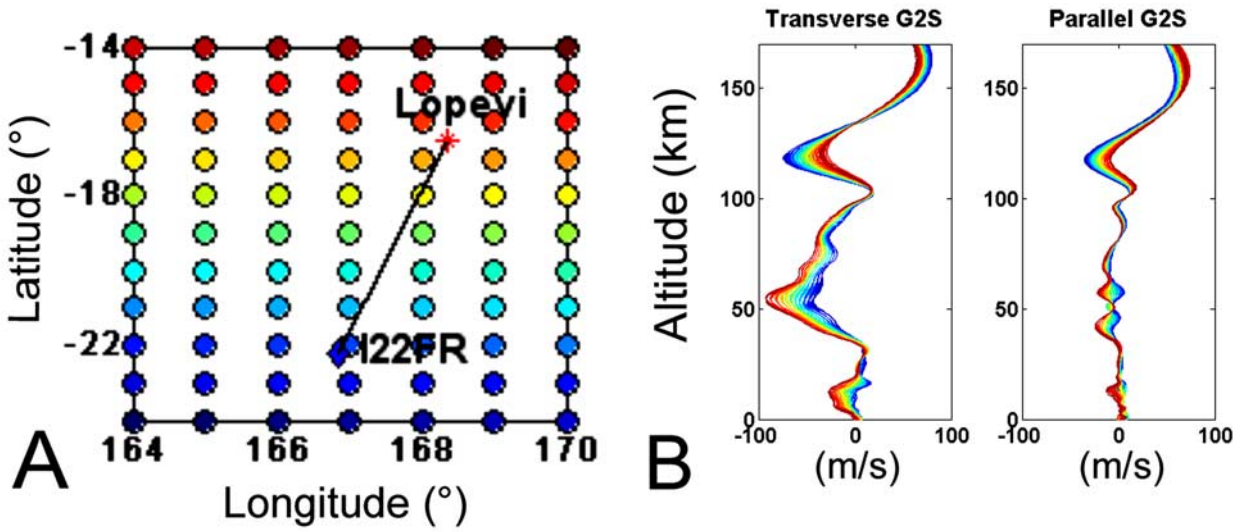

Figure 6. Grid of atmospheric profiles used for simulation. (a) Spatial grid with a step resolution of 1°. At each node of the grid, G2S profiles are given from ground to 170 km height. (b) Superposition of the 88 G2S parallel and transverse winds considering propagation from Lopevi to I22FR on 8 June 2003.

of the zonal stratospheric wind with season. Compared to the true bearing, the largest azimuth deviations occur as expected in July and January, when the strongest zonal winds are observed. Figure 7 also shows a dissymmetry in the amplitude of deviation (+5° in July and −10° in January). Because of a different direction of propagation, the amplitude of the azimuth deviation is smaller for Yasur.

[17] Comparison of the predicted azimuth deviations obtained with G2S and HWM-93 models shows similar seasonal trends (Figure 7a). However, because the HWM-93 empirical model only takes into account the climatological amplitudes and phases of the most basic weather patterns, simulations do not match well the observations. In particular, the azimuth deviation is significantly undervalued. The largest discrepancies reach 5°–7° in January–February. A better match is obtained using the more realistic G2S model which includes both the synoptic-scale meteorology in the troposphere and stratosphere and the complete geomagnetic, solar forcing and modulations of the general circulation and tides above 100 km. Although the bias in azimuth still remains in the order of 3°–5°, the seasonal azimuth fluctuations are reasonably well predicted by the G2S specifications even down to the timescale of a few days. Accounting for the tidal variability of the atmosphere, significant dispersion in azimuth is noted. From time to time, the observed and G2S-predicted dispersions in azimuth are of the same order (2°–3°).

[18] Depending on the prevailing winds, the propagating rays are refracted in the stratosphere or in the thermosphere, and reach the station after two or three bounces. For the Yasur volcano, stratospheric returns occur during the austral winter. During that season, the prevailing westward winds allow the formation of a stratospheric waveguide below ~40 km height (Figure 7b). Because of the dominant semidiurnal wind fluctuations around 120 km (Figure 5), turning heights of thermospheric paths oscillate between ~115 km at 0600 and 1800, and ~120 km at 0000 and 1200 UT. However, considering the relative high-frequency content of the signals (Figure 4), thermospheric arrivals are unlikely because of severe absorption in the upper atmosphere [*Sutherland and Bass*, 1996]. Because rays from Lopevi propagate almost in a direction perpendicular to the dominant zonal winds, the increase of the effective sound speed is not strong enough to favor stratospheric returns. Thus most of the rays return back to the ground after being refracted in the thermosphere (Figure 7c). The relative low-frequency content of the detected signals is compatible with this phase identification. Between November and March, only few rays are refracted in the stratopause.

[19] To summarize, according to the measured phase velocities and the simulation results, two dominant waveguides are predicted: (1) thermospheric phases from Lopevi refracted below 115–120 km and (2) stratospheric phases from Yasur refracted below 40–50 km. In the range of uncertainties of the measurements, a satisfactory predicted azimuth is obtained for Yasur, whereas for Lopevi a shift of some degrees has to be explained.

4.2. Influence of the Atmospheric Tides

[20] The influence of the solar heating driven diurnal and semidiurnal migrating tides in the mesosphere and lower thermosphere on both the azimuth deviation and the wave attenuation are also visible. Figure 8 presents the diurnal variations of the number of detections. Statistics are correlated to the daily fluctuations of the wind-related noise. The highest value of the noise level at 1 Hz is obtained during day time when the local wind speed reaches ~5 m/s (0000 UT corresponds to 1100 local time). As a result, due to the low amplitude of the signals, the number of detections significantly decreases during the day time. There is no signal from Lopevi from 0900 to 1200 UT although the wind-noise remains at a low level. As seen from Figure 7, rays refract at greater altitudes near 0000 and 1200 UT, thus are subject to increased attenuation. The lack of detection around 1200 UT can be explained by the strong attenuation in the upper atmosphere where the additional

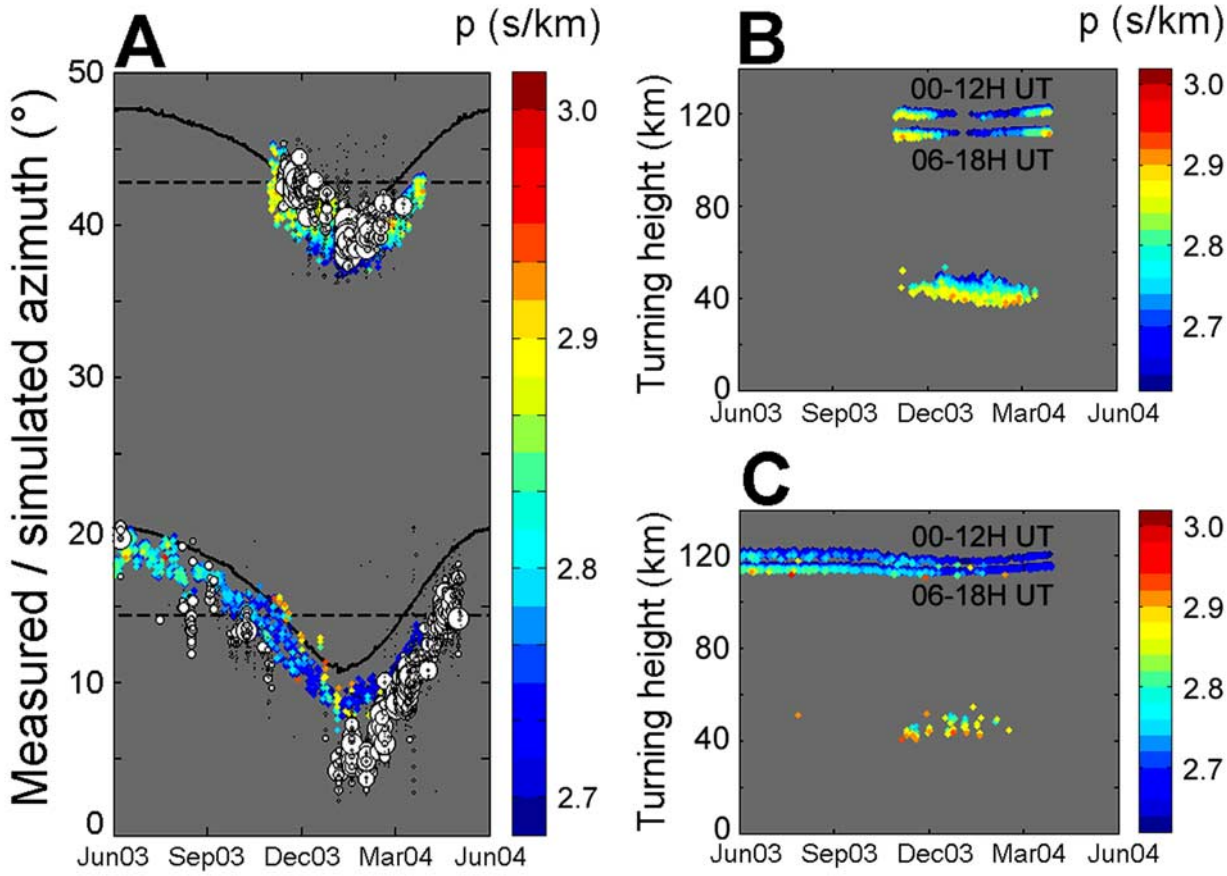

Figure 7. Results of propagation modeling. (a) Comparison between predicted/measured azimuths for Lopevi (bottom) and Yasur (top). Dashed lines are the true azimuths, white dots are the PMCC detections, black solid curves are the predicted azimuths for the MSIS/HWM model, and colored dots are the predicted azimuths derived from the G2S atmospheric profiles. Color refers to the ray parameter. (b and c) Predicted turning heights for Yasur and Lopevi, respectively.

absorption due to the difference in travel paths between 115 and 120 km is about 40 dB at 0.5 Hz (Figure 9). Earlier research by *Rind and Donn* [1975] dealing with atmospheric tidal circulation already pointed out such observations. On the other side, from 0600 to 1900 UT, the number of detections from Yasur is roughly constant since stratospheric paths are less sensitive to tidal variations of the winds, and the attenuation is in addition very weak (about 10^{-3} dB/km).

[21] The azimuth deviation mainly depends on the strong seasonal changes of the stratospheric winds. However, the tidal variability of the upper atmosphere also affects in a second-order the deflection of the ray direction. With a shift of 3°–4° between the observed and predicted seasonal azimuth deviation, the semidiurnal oscillations of the detected azimuths are in accordance with the G2S-predicted sine variations (Figure 10). Such deflections have already been pointed out by *Garcés et al.* [2002].

4.3. Probing High-Altitude Winds

[22] As for results from climatologies versus NWP data, it is important to consider that during certain seasons, primarily equinox and location (e.g., high and middle latitudes), the instantaneous atmospheric conditions in the lower atmosphere will deviate much from the climatological average. It is straightforward to evaluate the benefits of using comprehensive set ground truth events which covers all seasons and latitude ranges. In the global NWP specifications, transient mesoscale gravity waves are not individually resolved. Thus, one part of the observed discrepancies between the observations and the theory may be attributable to atmospheric gravity wave phenomena filtered out from the models. The impact of filtering out these perturbations remains a topic of active scientific investigation. More likely, either the undervaluation of the wind speed between the stratopause and the lower thermosphere, or the inaccuracy of the current predictions of stratospheric wind velocities in NWP data (e.g., ECMWF, NASA/NOAA), could explain the largest part of these discrepancies. Given the advanced state of the NWP specifications included in the G2S system, it is assumed that the wind fields below 55 km are essentially correct. One subject of atmospheric investigation is the development of inversion procedures to routinely specify the wind fields in the 55 to 120 km region.

[23] An example of such application is the dip in azimuth seen in mid-August. Figure 11 shows a decrease in the predicted azimuth of 2°–3° between 5 and 20 August 2003 whereas the observed variation reaches ~5°. During this time period, transverse wind reverses from −20 m/s to

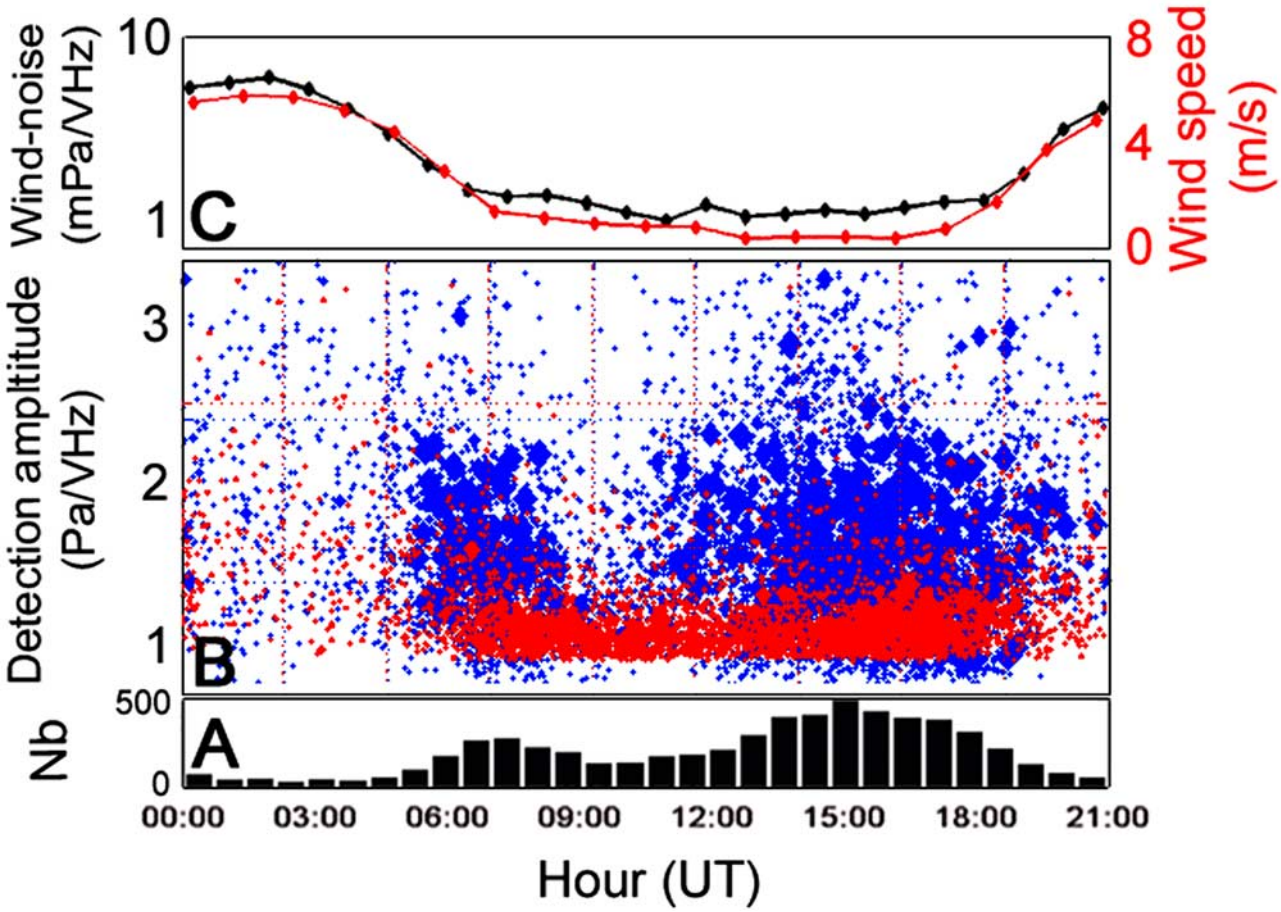

Figure 8. Statistics on the number of detections from June 2003 to May 2004 compared with wind-noise variation measured at I22FR. (a) Histograms on the number of detections versus time of day. (b) Measured amplitude of signals for Lopevi (in blue), and Yasur (in red) versus time of day. (c) Diurnal variations of infrasound noise level at 1 Hz (black) and hourly averaged wind speed (in red) measured at the central array element.

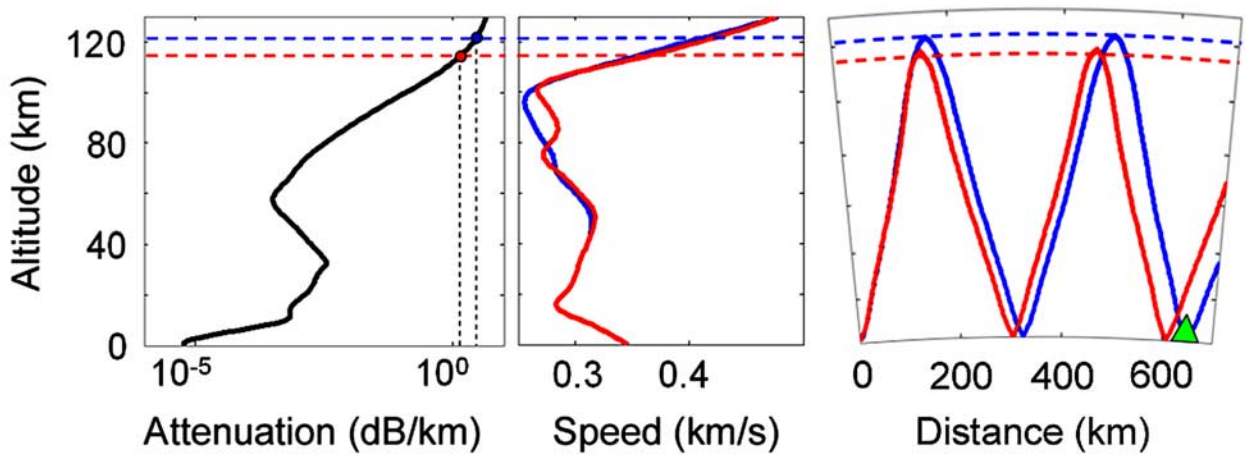

Figure 9. Atmospheric attenuation versus altitude for the frequency 0.5 Hz [*Sutherland and Bass*, 1996]. The total attenuation (in black) comprises rotational relaxation, classical and vibrational losses (O_2, N2, CO_2, and O3). Sound speed profiles corrected for the winds in the direction of propagation are given at 0000 (in blue) and 0600 UT (in red) on 1 January 2003. The corresponding ray traces indicate thermospheric paths with turning heights at 115 and 120 km.

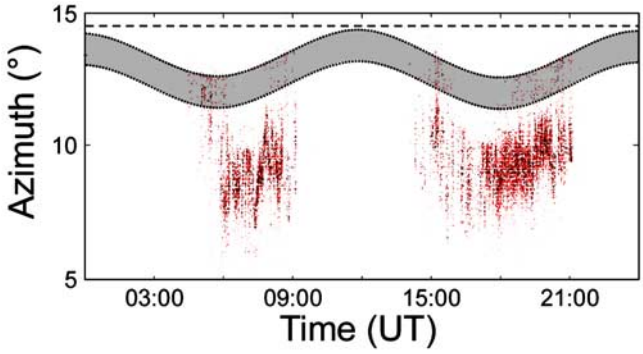

Figure 10. Typical semidiurnal azimuth deviation for signals from Lopevi (March 2004). Measurements (red dots) are compared with the G2S-predicted deviations of thermospheric paths for ray parameters ranging from 2.7 to 3 s/km (area between the two sine curves). The black solid dashed line indicates the true azimuth.

20 m/s in the 40 to 55 km region, breaking the seasonal trend in the azimuth variation. This reversal is the result of a significant quasi-stationary subtropical disturbance that formed over our region of interest in connection with a large stationary ridge in the polar winter stratospheric wind jet. These features and their evolution are clearly visible in global synoptic-scale maps generated from the stratospheric NWP analyses. Considering propagation of thermospheric paths, an extension of this large circulation cell up to 70 km would provide a good match between the measured and simulated azimuth deviation.

[24] Another example is given by Figure 12 where corrections of the G2S wind model are applied in order to reduce the negative shift in azimuth between measurements and simulations. The selected day is 15 January 2004 where the mismatch is the largest (Figures 12a and 12b). For the sake of simply, a uniform enhancement of the zonal wind component is applied in the 55 to 120 km region. Additional strategies for future work are discussed below. A correction factor of about 2 provides here good results. More systematically, from June 2003 to April 2004, an iterative algorithm is used for a daily correction of G2S winds. The procedure is initiating with the original G2S winds given at a time of day (1500 UT) corresponding to the maximum number of detections (Figure 8) and, step by step, winds are adjusted in order to reduce the bias between the observed and simulated azimuth deviations. The final results show that the G2S zonal winds between 50 and 110 km are underestimated by at least 20 m/s throughout the year (Figure 12c). The largest deviations are noted between November 2003 and February 2004 with differences reaching 50 m/s.

5. Conclusion

[25] Infrasonic waves from active volcanoes in Vanuatu are studied to evaluate the validity of atmospheric models. Considering a nearly southward propagation from the Lopevi volcano, the direction of propagation of the predicted thermospheric paths is subject to the reversibility of the transverse zonal winds. As a result, from summer to winter, an azimuth variation of $\sim$15° is noted. A 3-D paraxial ray-tracing modeling associated with the NRL-G2S climatological database are used to simulate the propagation. Over a period of near one year, comparison between the predicted and observed azimuth deviations shows similar seasonal trends. It is found that the seasonal azimuth fluctuations are reasonably well predicted by the G2S specifications even down to the timescale of a few days. Accounting for the tidal variability of the atmosphere, significant daily azimuth fluctuations are also observed. These results show that time and range-dependent propagation modeling can provide a good description of the general seasonal changes. However, systematic errors in the predicted azimuth deviation remain in the order of 3°–5°, with large discrepancies reaching 5°–7° in January–February 2004. From these comparisons, it is shown that the models used are inadequate for predicting accurate atmospheric changes above the stratosphere. More specifically, the mesospheric zonal winds are generally underestimated. We have demonstrated that the observed azimuth deviations provide a basis for investigation into the mathematics of geophysical inverse problems with infrasound for atmospheric remote sensing. These measurements also provide a powerful way to understand and quantify the relationship between infrasonic observables and the atmospheric specification problem.

[26] Further work could explore a more sophisticated inversion scheme for adjusting the G2S background fields. The choice of the scaled function correction, its range of application in altitude, and the addition of unknown atmospheric model parameters in the inversion procedure could in particular be considered. Theoretically, we can improve the accuracy and robustness of the atmospheric corrections by including additional infrasonic observables such as elevation angle of arrival, travel times, or even the measured

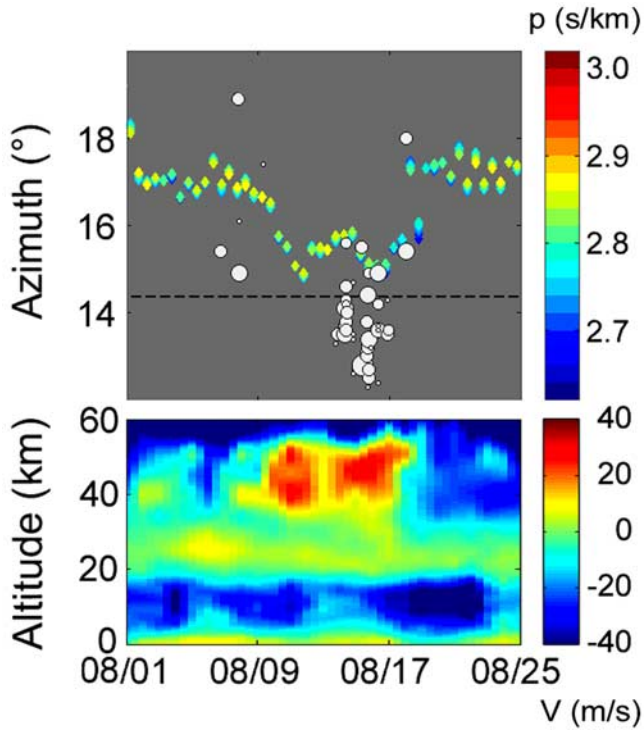

Figure 11. Detail in the predicted/measured azimuths for Lopevi from the 1 to 25 August 2003 and comparison with G2S transverse wind profiles at 0000 UT.

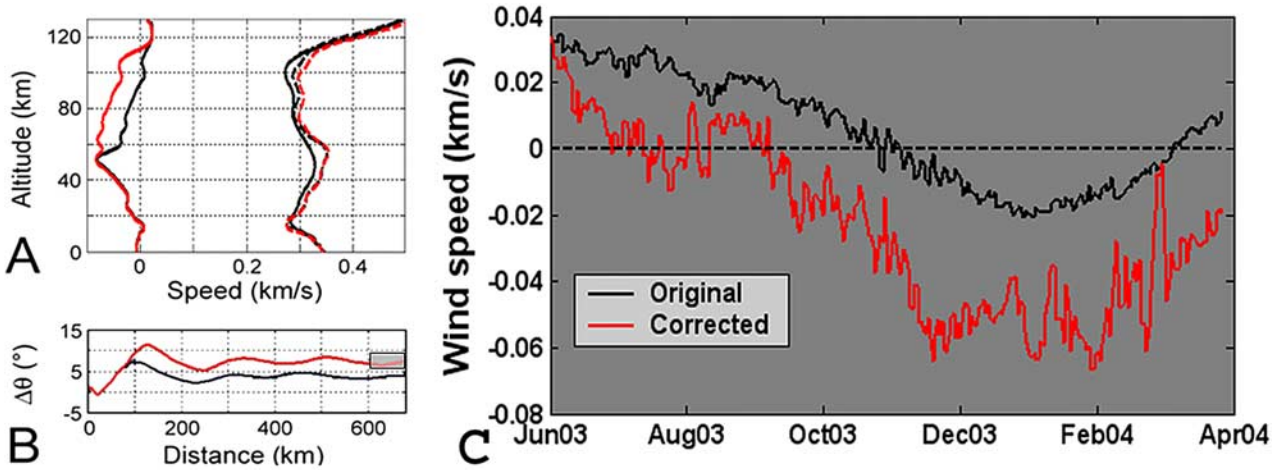

Figure 12. Correction of the G2S zonal wind averaged along the trajectory between Lopevi and I22FR. (a) Original and corrected winds on 15 January 2004 (black and red solid lines, respectively) (left side) and G2S sound speed profile (black solid line), effective sound speed (sound speed including winds in the direction of propagation) before and after correction (black and red dashed lines, respectively) (right side). (b) Predicted azimuth deviation without and with wind correction on 15 January 2004 (in black and red, respectively). The light patch indicates the range of measured azimuths at I22FR. (c) Original and corrected G2S winds averaged between 50 and 110 km, from June 2003 to April 2004 (in black and red, respectively).

azimuth deviations from nearby portable infrasound arrays. In particular, the elevation angle of the arrival, which is directly related to the ray parameter, is widely used in seismic and hydroacoustic geophysical inverse methods; however, for infrasonic signals the arrival elevations is currently difficult to measure. Perhaps by taking advantage of new signal processing methods, improved wind noise filters, and including additional array elements, it will be possible to obtain accurate arrival elevations that can be used in conjunction with travel time estimates to improve atmospheric estimation procedures. Continuing investigation into infrasonic signals from active volcanoes will certainly improve our understanding of the atmosphere and help to advance the development of automated source location procedures for operational infrasound monitoring.

[27] **Acknowledgments.** The authors are grateful to P. Herry for the time he spent helping us in the data analysis. Many thanks also to M. Garcés and P. F. Piserchia for their interests in this study and for the helpful discussions we had during the completion of this work. We would like to thank the NASA Goddard Space Flight Center, Global Modeling and Assimilation Office (GSFC-GMAO), and the NOAA National Centers for Environmental Prediction (NCEP) for providing the NWP data that went into the NRL-G2S atmospheric specifications. Funding was provided to NRL by the Office of Naval Research. Auxiliary support was also provided by Coordination de la Recherche Volcanologique and Ministère de l'Ecologie et Développement Durable to install instruments close to the Yasur volcano.

References

Alcoverro, B., and A. Le Pichon (2005), Design and optimization of a noise reduction system for infrasonic measurements using elements with low acoustic impedance, *J. Acoust. Soc. Am.*, *117*, 1717–1727, doi:10.1121/1.1804966.

Bass, H. E., L. C. Sutherland, A. J. Zuckerwar, D. T. Blackstock, and D. M. Hester (1995), Atmospheric absorption of sound: Further developments, *J. Acoust. Soc. Am.*, *97*, 680–683.

Bush, G. A., Y. A. Ivanov, S. N. Kulichkov, A. V. Kuchayev, and M. V. Pedanov (1989), Acoustic sounding of the fine structure of the upper atmosphere, *Izv. Akad. Sci. USSR Atmos. Oceanic Phys.*, Engl. Transl., *25*, 251–256.

Cansi, Y. (1995), An automatic seismic event processing for detection and location: The PMCC method, *Geophys. Res. Lett.*, *22*, 1021–1024.

Delclos, C., E. Blanc, P. Broche, F. Glangeaud, and J. L. Lacoume (1990), Processing and interpretation of microbarograph signals generated by the explosion of Mount St. Helens, *J. Geophys. Res.*, *95*, 5485–5494.

Donn, W. L. (1978), Exploring the atmosphere with sonic booms, *Am. Sci.*, *66*, 724–733.

Donn, W. L., and N. K. Balachandran (1981), Mount St. Helens eruption of 18 May 1980: Air wave and explosive yield, *Science*, *213*, 539–541.

Drob, D. P., and J. M. Picone (2000), Statistical performance measures of the HWM-93 and MSISE-90 empirical atmospheric models and the relation to infrasonic CTBT monitoring, in *Proceedings of the 22nd Annual DOD/DOE Seismic Research Symposium: Planning for Verification of and Compliance with the Comprehensive Nuclear Test Ban Treaty (CTBT), New Orleans, La., 13–15 Sept., 2000* [CD-ROM], paper 07_03, Dep. of Defense, Washington, D. C.

Drob, D. P., J. M. Picone, and M. A. Garcés (2003), Global morphology of infrasound propagation, *J. Geophys. Res.*, *108*(D21), 4680, doi:10.1029/2002JD003307.

Eissen, J. P., C. Blot, and R. Louat (1991), Chronology of the historic volcanic activity of the New Hebrides island arc from 1595 to 1991, *Rep. 2*, 69 pp., Geol. and Geophys., Inst. de Rech. pour le Dev., Nouméa, New Caledonia.

Evans, L. B., H. E. Bass, and L. C. Sutherland (1972), Atmospheric absorption of sound: Theoretical predictions, *J. Acoust. Soc. Am.*, *51*, 1565–1575.

Garcés, M. A., D. P. Drob, and J. M. Picone (2002), A theoretical study of the effect of geomagnetic fluctuations and solar tides on the propagation of infrasonic waves in the upper atmosphere, *Geophys. J. Int.*, *148*, 77–87.

Garcés, M. A., M. Willis, C. Hetzer, A. Le Pichon, and D. Drob (2004), On using ocean swells for continuous infrasonic measurements of winds and temperature in the lower, middle, and upper atmosphere, *Geophys. Res. Lett.*, *31*, L19304, doi:10.1029/2004GL020696.

Georges, T. M., and J. M. Young (1972), Passive sensing of natural acoustic gravity waves at the Earth's surface, in *Remote Sensing of the Troposphere*, edited by V. E. Derr, chap. 21, U.S. Gov. Print. Off., Washington, D. C.

Greenspan, M. (1959), Rotational relaxation in nitrogen, oxygen, and air, *J. Acoust. Soc. Am.*, *31*, 155–161.

Hagerty, M. T., S. Y. Schwartz, M. A. Garcés, and M. Protti (2000), Analysis of seismic and acoustic observations at Arenal Volcano, Costa Rica, 1995–1997, *J. Volcanol. Geotherm. Res.*, *101*, 27–65.

Hedin, A. E. (1991), Extension of the MSIS thermosphere model into the middle and lower atmosphere, *J. Geophys. Res.*, *96*, 1159–1172.

Hedin, A. E., et al. (1996), Empirical wind model for the upper, middle and lower atmosphere, *J. Atmos. Terr. Phys.*, *58*, 1421–1447.

Hedlin, M., M. A. Garcés, H. Bass, C. Hayward, G. Herrin, J. Olson, and C. Wilson (2002), Listening to the secret sounds of Earth's atmosphere, *Eos Trans. AGU*, *83*(48), 557, 564–565.

Herron, T. J., and I. Tolstoy (1968), Tracking jet stream winds from ground level pressure signals, *J. Atmos. Sci.*, *26*, 266–269.

Jones, M. J., J. P. Riley, and T. M. Georges (1986), A versatile three-dimensional Hamiltonian ray tracing program for acoustic waves in the atmosphere above irregular terrain, *Spec. Rep. PB87-172573*, Wave Propag. Lab., NOAA, Boulder, Colo.

Kanamori, H., J. Mori, and D. G. Harkrider (1994), Excitation of atmospheric oscillations by volcanic eruptions, *J. Geophys. Res.*, *99*, 21,947–21,961.

Kulichkov, S. N. (1992), Long-range propagation of sound in the atmosphere: A review, *Izv. Acad. Sci. USSR Atmos. Oceanic Phys.*, Engl. Transl., *28*, 253–269.

Lardy, M., R. Priam, and D. Charley (1999), Lopévi: Résumé de l'activité historique et de l'activité récente, *Rep. LAVE 77*, 5 pp., Geol. and Geophys., Inst. de Rech. pour le Dev., Nouméa, New Caledonia.

Le Pichon, A., M. A. Garcés, E. Blanc, M. Barthelemy, and D. P. Drob (2002a), Acoustic propagation and atmosphere characteristics derived from infrasonic waves generated by the Concorde, *J. Acoust. Soc. Am.*, *111*, 629–641.

Le Pichon, A., J. Guilbert, A. Vega, M. A. Garcés, and N. Brachet (2002b), Ground-coupled air waves and diffracted infrasound from the Arequipa earthquake of June 23, 2001, *Geophys. Res. Lett.*, *29*(18), 1886, doi:10.1029/2002GL015052.

Liszka, L., and A. Garcés (2002), Infrasonic observations of the Hekla eruption of February 26, 2000, *J. Low Freq. Noise Vib.*, *21*, 1–8.

McCall, G. J., R. W. LeMaitre, A. Malahoff, G. P. Robinson, and P. J. Stephenson (1970), The geology and geophysics of Ambrym Caldera, New Hebrides, *Bull. Volcanol.*, *34*, 681–696.

McClelland, L., T. Simkin, M. Summers, E. Nielsen, and T. C. Stein (1989), *Global Volcanism: 1975–1985*, Prentice-Hall, Upper Saddle River, N. J.

Morrissey, M. M., and B. A. Chouet (1997), Burst conditions of explosive volcanic eruptions recorded on microbarographs, *Science*, *275*, 1290–1293.

Picone, J. M., A. E. Hedin, D. P. Drob, and A. C. Aikin (2002), NRLMSISE-00 empirical model of the atmosphere: Statistical comparisons and scientific issues, *J. Geophys. Res.*, *107*(A12), 1468, doi:10.1029/2002JA009430.

Reed, J. W. (1987), Air pressure waves from Mount St. Helens eruptions, *J. Geophys. Res.*, *92*, 11,979–11,992.

Rind, D. (1977), Heating of the lower thermosphere by dissipation of acoustic waves, *J. Atmos. Terr. Phys.*, *39*, 445–456.

Rind, D. (1978), Investigation of the lower thermosphere results of ten years of continuous observations with natural infrasound, *J. Atmos. Terr. Phys.*, *40*, 1199–1209.

Rind, D., and W. L. Donn (1975), Further use of natural infrasound as a continuous monitor of the upper atmosphere, *J. Atmos. Sci.*, *32*, 1694–1704.

Ripepe, M., P. Poggi, T. Braun, and E. Gordeev (1996), Infrasonic waves and volcanic tremor at Stromboli, *Geophys. Res. Lett.*, *23*, 181–184.

Robin, C., and M. Monzier (1994), Volcanic hazards in Vanuatu, *Rep. 16*, 15 pp., Geol. and Geophys., Inst. de Rech. pour le Dev., Nouméa, New Caledonia.

Robin, C., J. P. Eissen, and M. Monzier (1993), Giant tuff cone and 12–km–wide associated caldera at Ambrym Volcano, Vanuatu, New Hebrides Arc, *J. Volcanol. Geotherm. Res.*, *55*, 225–238.

Simkin, T., and L. Siebert (1994), *Volcanoes of the World*, Geoscience, Tucson, Ariz.

Sutherland, L. C., and H. E. Bass (1996), Atmospheric absorption in the atmosphere at high altitudes, paper presented at the 7th Long-range Sound Propagation Symposium, Ecole Centrale de Lyon, Lyon, France.

Tahira, M., M. Nomura, Y. Sawada, and K. Kamo (1996), Infrasonic and acoustic-gravity waves generated by the Mount Pinatubo eruption of June 15, 1991, in *Fire and Mud: Eruptions and Lahars of Mount Pinatubo, Philippines*, edited by C. G. Newhall and R. S. Punongbayan, pp. 601–613, Univ. of Wash. Press, Seattle.

Vergniolle, S., and G. Brandeis (1996), Strombolian explosions: A large bubble breaking at the surface of a lava column as a source of sound, *J. Geophys. Res.*, *101*, 433–448.

Vergniolle, S., M. Boichu, and J. Caplan-Auerbach (2004), Acoustic measurements of the 1999 basaltic eruption of Shishaldin Volcano, Alaska: 1) Origin of Strombolian activity, *J. Volcanol. Geotherm. Res.*, *137*, 109–134.

Virieux, J., and V. Farra (1991), Ray tracing in 3D complex isotropic media: An analysis of the problem, *Geophysics*, *56*, 2057–2069.

Virieux, J., N. Garnier, E. Blanc, and J.-X. Dessa (2004), Paraxial ray tracing for atmospheric wave propagation, *Geophys. Res. Lett.*, *31*, L20106, doi:10.1029/2004GL020514.

Vivas Veloso, J. A., D. R. Christie, P. Campus, M. Bell, T. L. Hoffman, A. Langlois, P. Martysevich, E. Demirovik, J. Carvalho, and A. Kramer (2002), Status report on the establishment of the Comprehensive Nuclear Test Ban Treaty (CTBT) International Monitoring System (IMS) infrasound network, *J. Acoust. Soc. Am.*, *112*, 2352.

Warden, A. J. (1963), Interim report on the 1963 Lopevi eruption, *Rep. DV32*, 52 pp., Geol. Surv. Dep., Port Vila, Vanuatu.

Wilson, C. R., and R. B. Forbes (1969), Infrasonic waves from Alaskan volcanic eruption, *J. Geophys. Res.*, *74*, 4511–4522.

P. Bani and M. Lardy, IRD, BPA5, 98848 Noumea cedex, New Caledonia.

E. Blanc and A. Le Pichon, CEA/DASE/LDG, BP12, F-91680 Bruyères-le-Châtel, France. (alexis.le-pichon@cea.fr)

J. X. Dessa, LGM-IPGP, 4 place Jussieu, F-75252 Paris Cedex 05, France.

D. Drob, E.O. Hulburt Center for Space Research, Naval Research Laboratory, 4555 Overlook Avenue, Washington, DC 20375, USA.

S. Lambotte, EOST-IPGS, 5 rue René Descartes, F-67084 Strasbourg cedex, France.

S. Vergniolle, LDSG-IPGP, 4 place Jussieu, F-75252 Paris Cedex 05, France.